ARTICLES

Hydrothermal Synthesis of Zn_2SnO_4 Nanorods in the Diameter Regime of Sub-5 nm and Their Properties

Hongliang Zhu,*,†,‡ Deren Yang,‡ Guixia Yu,† Hui Zhang,‡ Dalai Jin,† and Kuihong Yao†

Center of Materials Engineering, Zhejiang Sci-Tech University, Xiasha University Town, Hangzhou 310018, China, and State Key Lab of Silicon Materials, Zhejiang University, Hangzhou 310027, China

Received: January 16, 2006; In Final Form: March 3, 2006

Single crystalline Zn_2SnO_4 (ZTO) nanorods 2−4 nm in diameter and around 20 nm in length were successfully synthesized by a simple hydrothermal process with use of hydrazine hydrate as an alkaline mineralizer instead of NaOH or $NH_3{\cdot}H_2O$. By analyzing the UV−vis diffuse reflectance spectrum, the optical band gap (E_g) of the nanorods was found to be 3.87 eV, which indicates a blue shift of 0.27 eV from that of bulk ZTO (3.6 eV). In situ high-temperature X-ray diffraction was employed to study the thermal expansion coefficient and the variation of lattice parameter with temperature of the product. Furthermore, we discussed the chemical mechanism and key factors to the hydrothermal formation of the sub-5 nm ZTO nanorods.

1. Introduction

One-dimensional (1-D) nanostructures of binary semiconducting oxides, such as ZnO and SnO_2, have attracted great attention due to their prominent properties, and their potential applications.[1−4] Ternary oxide spinel zinc stannate, Zn_2SnO_4 (ZTO), is also an interesting semiconducting material with the same band gap energy as that of SnO_2 (E_g = 3.6 eV).[5] ZTO has promising applications in photovoltaic devices, combustible gases and humidity detection, photoelectrochemistry, functional coatings, and transparent conducting electrodes due to its high electron mobility, high electrical conductivity, and low visible absorption.[6−13] ZTO nanostructures may show better properties than those of ZnO and SnO_2, but they are still less studied. Herein, we report an additive-free hydrothermal route to the sub-5 nm single crystalline ZTO nanorods, using hydrazine hydrate ($N_2H_4{\cdot}H_2O$) as an alkaline mineralizer instead of NaOH or $NH_3{\cdot}H_2O$. When the dimensions of semiconducting nanostructures are smaller than or comparable to their corresponding exciton Bohr radius, they display strong quantum confinement effects and novel physical properties different from those of their bulk materials.[14] Therefore, the preparation of ultrafine semiconducting nanostructures in the diameter regime of sub-5 nm has become very significant.

In recent years, ZTO nanostructures have been prepared by the thermal evaporation method,[15−19] mechanical grinding,[20] and high-temperature solid reaction.[21] Compared with the above processes, the hydrothermal method has sparked much interest due to operational simplicity, cost-efficiency, and the capability for large-scale production. Wu and co-workers reported hydrothermal synthesis of ZTO crystals.[22] However, to the best of our knowledge, hydrothermal synthesis of ZTO nanostructures has not been reported. The major advantage of the hydrothermal process presented here is to bring down the diameters of the ZTO nanocrystallines to the sub-5 nm regime. Such ZTO nanorods display a noticeable blue-shift from the band gap of the bulk ZTO crystal.

2. Experimental Section

All reagents were of analytical grade without further purification. In a typical experiment, $ZnCl_2$ (1.7408 g, 12.8 mmol), $SnCl_4{\cdot}5H_2O$ (2.2400 g, 6.4 mmol), and $N_2H_4{\cdot}H_2O$ (2.5600 g, 51.2 mmol) were added to deionized water (160 mL) with stirring, meaning that the mole ratio of $ZnCl_2$:$SnCl_4$:$N_2H_4{\cdot}H_2O$ was 2:1:8. $N_2H_4{\cdot}H_2O$ immediately reacted with $ZnCl_2$ and $SnCl_4$ in the solution, and a slurrylike white precipitate of the hybrid complex was formed. After 10 min of stirring the solution was transferred into a Teflon-lined stainless steel autoclave of 200 mL capacity and then sealed. The autoclave was maintained at 250 °C for 24 h and cooled naturally to room temperature. The product formed at the bottom of the autoclave was centrifuged, filtered out, and rinsed with alcohol and deionized water several times. Finally, the product was dried at 60 °C for 1 h in air.

The X-ray diffraction (XRD) pattern was obtained on a Thermo ARL XTRA X-ray diffractometer with Cu Kα radiation (λ = 1.54178 Å). In situ XRD characterization was performed in a high-temperature attachment of the X-ray diffractometer. Transmission electron microscopy (TEM) observation was performed with a JEOL JEM 2010 high-resolution transmission electron microscope (HRTEM) operated at 200 kV. The UV−vis diffuse reflectance spectrum (DRS) was obtained from a Perkin-Elmer Lambda 900 UV−vis spectroscopy machine. The precursor was characterized by Fourier transform infrared (FT-IR) spectroscopy on a Perkin-Elmer Spectrum One FT-IR machine by using the KBr pellets method.

* To whom correspondence should be addressed. Phone/Fax: +86 571 86843266. E-mail: webmaster@51yq.com.
† Center of Materials Engineering, Zhejiang Sci-Tech University.
‡ State Key Lab of Silicon Materials, Zhejiang University.

10.1021/jp060304t CCC: $30.25
Published on Web 03/31/2006

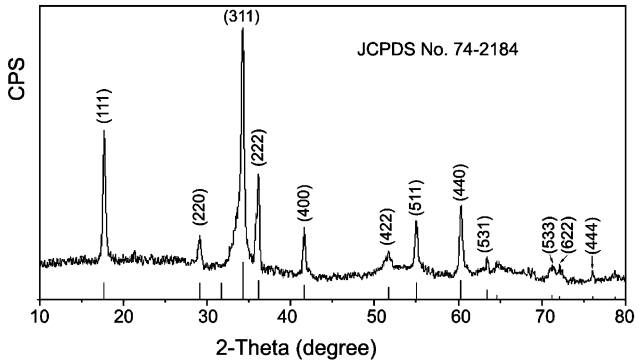

Figure 1. XRD pattern of the sub-5 nm ZTO nanorods.

3. Results and Discussion

Figure 1 shows the XRD pattern of the ZTO nanorods. All the peaks can be indexed to cubic ZTO with lattice constants: $a = 8.65$ Å, which is in good agreement with the values from the standard card (JCPDS No. 74-2184). Interestingly, the relative intensity of the (111) peak is ~56%, which is much stronger than that of the (111) peak in the standard card (36.4%). The (222) peak shows a similar feature to the (111) peak, whereas the relative intensities of other peaks do not deviate much from their corresponding values in the standard card. Therefore, we can conclude that the ZTO nanorods might have a preferential [111] growth direction. In addition, ZTO crystals were obtained by a comparative experiment with NaOH as a mineralizer under the same condition, and their XRD pattern is similar to that of Figure 1.

A JEOL JEM 2010 high-resolution transmission electron microscope (HRTEM) was used to characterize the ZTO nanorods and the ZTO crystals, and typical TEM images are shown in Figure 2. Figure 2a is a low-magnification TEM image of the ZTO nanorods with the selected area electron diffraction (SAED) pattern. Figure 2a reveals that the product is composed of the homogeneous ultrafine nanorods. The SAED "halo" ring pattern taken from several ZTO nanorods confirms that the product is crystallized; the two rings correspond well to the {311} and {422} planes of ZTO, respectively. Figure 2b clearly shows that the product consists of rodlike nanostructures 2−4 nm in diameter and about 20 nm in length, which are called "sub-5 nm ZTO nanorods" in this paper. The ZTO nanorods were investigated by HRTEM in detail, and all nanoparticles showed uniform lattice fringes, meaning that no amorphous product was formed. Figure 2c is the HRTEM image of a single ZTO nanorod, which clearly indicates that the ZTO nanorod is structurally uniform single crystalline in nature. The lattice fringes with a d spacing of about 0.32 nm, corresponding to the {110} planes of ZTO (JCPDS No. 74-2184), are found in Figure 2c. Therefore, the lateral direction (nanorod diameter) and vertical direction (nanorod length) of the ZTO nanorods are the [110] direction and [111] direction, respectively. As discussed above, we attribute the formation of the nanorods to their preferential growth along the [111] direction. Moreover, Figure 2c shows that the ZTO nanorods are covered with amorphous ultrathin films. Perhaps some diffused rings of the SAED pattern which may be corresponding to the amorphous ZTO come from the amorphous ultrathin films. Figure 2d is the TEM image of the ZTO crystals (ZTO cubes 500 nm in width), which is consistent with the result reported by Wu et al.[22]

ZTO is an important wide band gap semiconducting ternary oxide with a band gap of 3.6 eV.[5] For ultrafine ZTO nanoparticles, the quantum confinement effect is expected, and the band gap is shifted to a higher energy. Herein, the band gaps of the ZTO nanorods and the ZTO crystals are studied by UV−vis

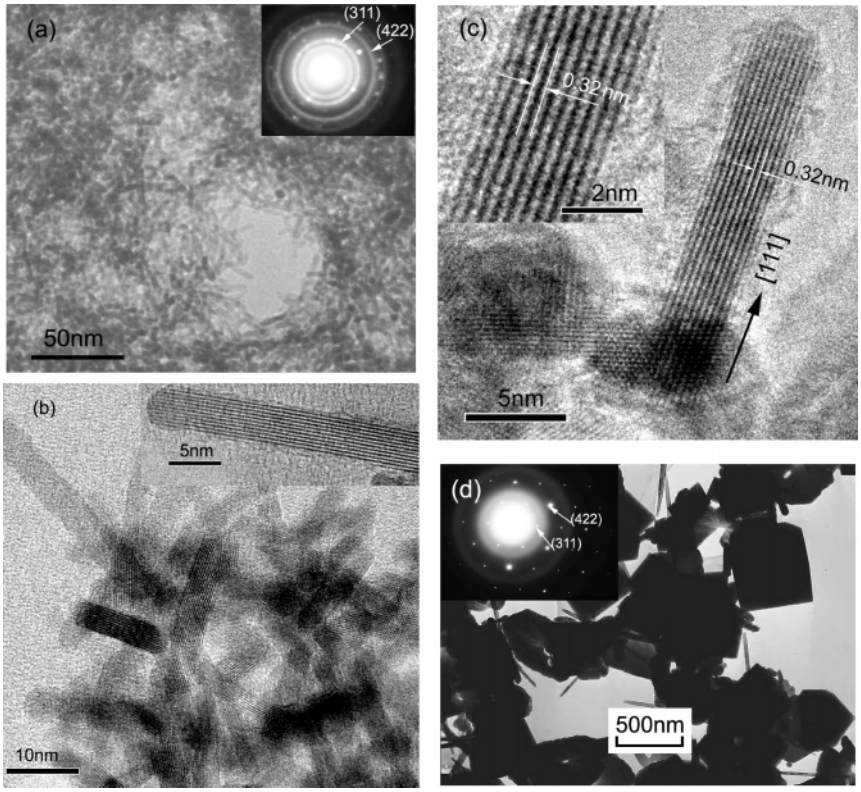

Figure 2. TEM images of the ZTO nanorods and the ZTO crystals: (a) the low-magnification image and SAED pattern of the ZTO nanorods, (b) image of several ZTO nanorods, (c) HRTEM image of a single ZTO nanorod, and (d) image and SAED pattern of the ZTO crystals.

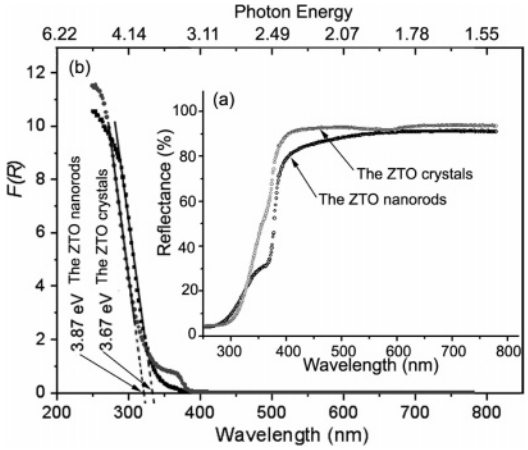

Figure 3. (a) DRS spectrum of the ZTO nanorods and the ZTO crystals and (b) plots of $F(R)$ vs wavelength.

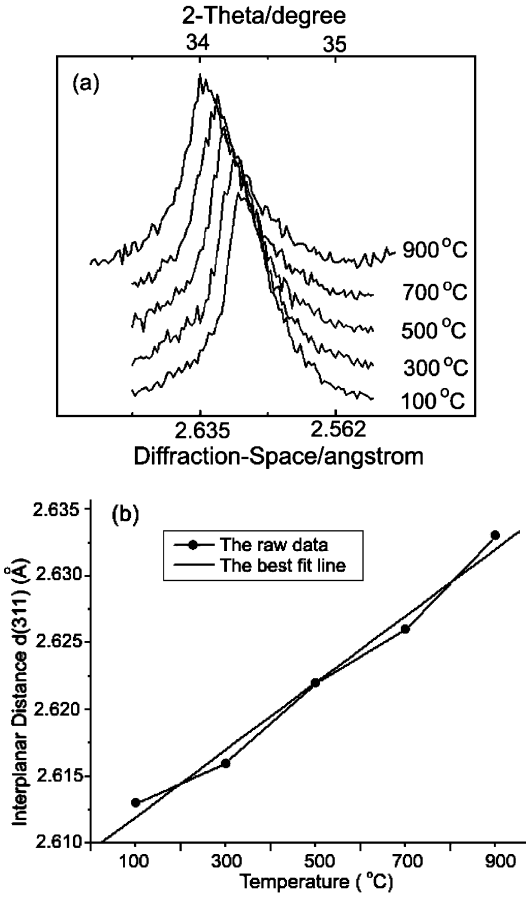

Figure 4. Diagram of the thermal expansion coefficient along [311] of the ZTO nanorods: (a) in situ XRD pattern of the peak of the {311} plane and (b) d(311) vs temperature.

diffuse reflectance spectroscopy (DRS). Furthermore, the Kubelka−Munk function, $F(R) = (1 - R)^2/2R$, is used to determine the band gaps by analyzing the DRS results. Figure 3 shows the DRS spectra of the ZTO nanorods and the ZTO crystals, and their plots of $F(R)$ vs wavelength. As shown in Figure 3b, the band gaps of the nanorods and the crystals are 3.87 (321 nm) and 3.67 eV (339 nm), respectively. Compared with the ZTO crystals (3.67 eV), the sub-5 nm ZTO nanorods show a significant blue shift. Figure 3a reveals that ZTO exhibits low visible absorption. ZTO can be used as a good transparent conducting oxide semiconductor for transparent electrodes.

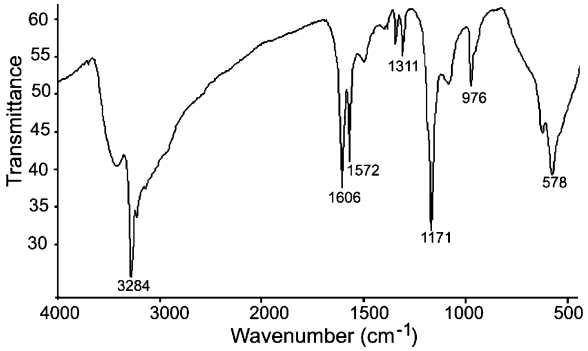

Figure 5. FT-IR spectrum of the precursor (the white precipitate).

The lattice parameter and thermal expansion are two important material properties that are strongly correlated to many thermophysical properties and advanced applications. In situ XRD measurement may be one of the most precise methods to measure thermal expansion coefficients of materials.[23] The in situ high-temperature XRD patterns of the peak at 34.36° corresponding to the {311} plane, the strongest peak of the standard card (JCPDS No. 74-2184), are presented in Figure 4a. The plot of the interplanar distance d(311) vs temperature is shown in Figure 4b, which reveals an almost linear thermal expansion behavior. The thermal expansion coefficient is given by

$$\alpha_T = \mathrm{d}l_T/(l_T\,\mathrm{d}T), \tag{1}$$

where l_T is length at temperature T. According to the linear relationship shown in Figure 4b, the thermal expansion coefficient of ZTO along [311] ($\alpha_{[311]}$) is 25.00×10^{-6} K^{-1}. Consequently, the thermal expansion coefficient along the a-, b-, and c-axis ($\alpha_{[100]}$) is 7.55×10^{-6} K^{-1} due to the cubic structure of ZTO. Therefore, the relation of the lattice parameter vs temperature is given by

$$a_T = 8.65 + (7.55 \times 10^{-6})T, \tag{2}$$

where T is temperature.

The most important advantage of this synthesis route is to bring down the diameters of the ZTO nanostructures to the sub-5 nm regime, using hydrazine hydrate as the alkaline mineralizer instead of NaOH or $NH_3{\cdot}H_2O$. In traditional hydrothermal processes with NaOH as the mineralizer, the chemical mechanism for hydrothermal formation of the ZTO crystals can be expressed as follows:

$$2ZnCl_2 + SnCl_4 + 8NaOH \rightarrow 2Zn(OH)_2\downarrow + Sn(OH)_4\downarrow + 8NaCl \tag{3}$$

$$2Zn(OH)_2 + Sn(OH)_4 \rightarrow Zn_2SnO_4 + 4H_2O \tag{4}$$

Prior to the hydrothermal process, $Zn(OH)_2$ and $Sn(OH)_4$ precipitates are formed via reaction 3. Reaction 4 represents the formation of the ZTO crystals from the $Zn(OH)_2$ and $Sn(OH)_4$ precipitates during the hydrothermal stage. The sizes of the precipitates have important roles in the size of ZTO crystals. Consequently, it is difficult to hydrothermally synthesize ZTO crystals of small size (Figure 2d). But when hydrazine hydrate is used as the mineralizer, $N_2H_4{\cdot}H_2O$ acts as a ligand, coordinating with Sn ions (6-coordinate) and Zn ions (4-coordinate). Consequently, the $(ZnCl_2)_m(N_2H_4)_n(SnCl_4)_y$ complex clusters are formed. Then, the complex clusters are agglomerated into the slurrylike white precipitate. To verify this point, the slurrylike

precipitate was characterized by FT-IR, and its FT-IR spectrum is shown in Figure 5. Figure 5 clearly exhibits vibration bands corresponding to hydrazine molecules,[24] suggesting that the complex precipitate was formed between N_2H_4 and the inorganic salts ($ZnCl_2$ and $SnCl_4$). The sharp peak at 3284 cm^{-1} is assigned to the N−H stretching vibration; two sharp peaks at 1606 and 1572 cm^{-1} are assigned to the NH_2 scissors. The wag and twist bands appeared at 1311 and 1171 cm^{-1}, respectively. The peak at around 976 cm^{-1} is often caused by the stretching band ν(N−N) of bridging H_2N-NH_2 between two metal ions.[25] The possible chemical mechanism of the formation of the ZTO nanorods can be expressed as follows:

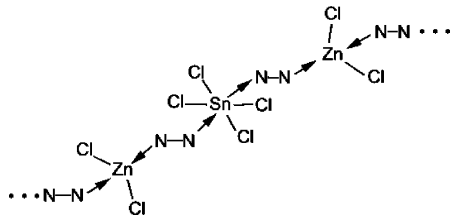

(5)

$$m\mathrm{ZnCl_2} + n\mathrm{N_2H_4} + y\mathrm{SnCl_4} \rightarrow (\mathrm{ZnCl_2})_m(\mathrm{N_2H_4})_n(\mathrm{SnCl_4})_y \quad (6)$$

$$(\mathrm{ZnCl_2})_m(\mathrm{N_2H_4})_n(\mathrm{SnCl_4})_y \rightarrow m\mathrm{Zn^{2+}} + n\mathrm{N_2H_4} + y\mathrm{Sn^{4+}} + (2m + 4y)\mathrm{Cl^-} \quad (7)$$

$$3\mathrm{N_2H_4} + 4\mathrm{H_2O} \rightarrow 4\mathrm{NH_4OH} + \mathrm{N_2} \quad (8)$$

$$2\mathrm{Zn^{2+}} + 8\mathrm{NH_4OH} + \mathrm{Sn^{4+}} \rightarrow \mathrm{Zn_2SnO_4} + 8\mathrm{NH_4^+} + 4\mathrm{H_2O} \quad (9)$$

Prior to the hydrothermal stage, the $(ZnCl_2)_m(N_2H_4)_n(SnCl_4)_y$ clusters are formed via reaction 6, and then the clusters are agglomerated into the slurrylike white precipitate. As represented in reaction 7, the $(ZnCl_2)_m(N_2H_4)_n(SnCl_4)_y$ clusters undergo dissociation. In the reaction 8 OH^{-1} ions are formed via the dissociation of N_2H_4 into NH_3 and N_2. Reaction 9 represents the formation of ZTO via the reaction between metal ions (Zn^{2+} and Sn^{4+}) and OH^- ions formed in reaction 8. We believe that the dissociation of N_2H_4 from the complex (reaction 7), the formation of OH^- (reaction 8), and the formation of the ZTO nanorods occur at local regions of the complex cluster, Therefore, during the hydrothermal stage the ultrafine ZTO nanorods with a diameter of 2−4 nm were formed.

Hydrazine hydrate, hydrothermal temperature, and the mole ratio of $ZnCl_2$:$SnCl_4$ are three key factors for hydrothermal formation of the sub-5 nm ZTO nanorods. As shown in Figure 2d, ZTO crystals instead of the sub-5 nm nanorods were formed when NaOH was used as the mineralizer. The final solution in the Experimental Section was hydrothermally processed at 150, 200, 250, and 280 °C. The products processed at 150 and 200 °C were amorphous and those processed at 250 and 280 °C were crystalline ZTO nanorods. In addition, different mole ratios of $ZnCl_2$:$SnCl_4$ were adopted, and pure ZTO nanorods were obtained when the mole ratio was 2:1.

4. Conclusions

Zn_2SnO_4 (ZTO) nanorods (2−4 nm in diameter and about 20 nm in length) were successfully synthesized by a simple hydrothermal process with hydrazine hydrate as an alkaline mineralizer. The optical band gap (E_g) of the ZTO nanorods was found to be 3.87 eV by analyzing the UV−vis diffuse reflectance spectrum, which shows a significant blue shift of 0.27 eV from that of bulk ZTO (3.6 eV). The thermal expansion coefficient, and the relationship between the lattice parameter of ZTO and temperature ($a_T = 8.65 + (7.55 \times 10^{-6})T$) were obtained from in situ XRD patterns. Prior to the hydrothermal process, hydrazine hydrate immediately reacted with $ZnCl_2$ and $SnCl_4$ to form a slurrylike white precipitate of the complex clusters, which have important roles in the formation of the sub-5 nm ZTO nanorods. Hydrazine hydrate, hydrothermal temperature, and the mole ratio of $ZnCl_2$:$SnCl_4$ are three key factors for hydrothermal formation of the ultrafine nanorods.

Acknowledgment. The author would like to acknowledge the support of the Natural Science Foundation of China (No. 50442025). We also thank Prof. Yaowu Zeng for TEM measurements.

References and Notes

(1) Huang, M. H.; Mao, S.; Feick, H.; Yan, H.; Wu, Y.; Kind, H.; Weber, E.; Russo, R.; Yang, P. *Science* **2001**, *292*, 1897.
(2) Gao, P.; Wang, Z. L. *J. Phys. Chem. B* **2002**, *106*, 12653.
(3) Wang, Y.; Lee, J. Y.; Deivaraj, T. C. *J. Phys. Chem. B* **2004**, *108*, 13589.
(4) Zhang, H.; Yang, D.; Ma, X.; Que, D. *J. Phys. Chem. B* **2005**, *109*, 17055.
(5) Coutts, T. J.; Young, D. L.; Li, X.; Mulligan, W. P.; Wu, X. *J. Vac. Sci. Technol. A* **2000**, *18*, 2646.
(6) Cun, W.; Wang, X. M.; Zhao, J. C.; Mai, B. X.; Sheng, G. Y.; Peng, P. A.; Fu, J. M. *J. Mater. Sci.* **2002**, *37*, 2989.
(7) Yu, J. H.; Choi, G. M. *Sens. Actuators, B* **2001**, *72*, 141.
(8) Moon, W. J.; Yu, J. H.; Choi, G. M. *Sens. Actuators, B* **2001**, *80*, 21.
(9) Yu, J. H.; Choi, G. M. *J. Electrochem. Soc.* **2001**, *148*, G307.
(10) Stambolova, I.; Konstantinov, K.; Kovacheva, D.; Peshev, P.; Donchev, T. *J. Solid State Chem.* **1997**, *128*, 305.
(11) Hashemi, T.; Al-Allak, H. M.; Illingsworth, J.; Brinkman, A. W.; Woods, J. *J. Mater. Sci. Lett.* **1990**, *9*, 776.
(12) Ginley, D. S.; Bright, C. *MRS Bull.* **2000**, *25*, 15.
(13) Minami, T. *Semicond. Sci. Technol.* **2005**, *20*, S35.
(14) Petroff, P. M.; Lorke, A.; Imamoglu, A. *Phys. Today* **2001**, *54*, 46.
(15) Jie, J.; Wang, G.; Han, X.; Fang, J.; Yu, Q.; Liao, Y.; Xu, B.; Wang, Q.; Hou, J. G. *J. Phys. Chem. B* **2004**, *108*, 8249.
(16) Chen, H.; Wang, J.; Yu, H.; Yang, H.; Xie, S.; Li, J. *J. Phys. Chem. B* **2005**, *109*, 2573.
(17) Wang, L.; Zhang, X.; Liao, X.; Yang, W. *Nanotechnology* **2005**, *16*, 2928.
(18) Wang, J. X.; Xie, S. S.; Gao, Y.; Yan, X. Q.; Liu, D. F.; Yuan, H. J.; Zhou, Z. P.; Song, L.; Liu, L. F.; Zhou, W. Y.; Wang, G. *J. Cryst. Growth* **2004**, *267*, 177.
(19) Wang, J. X.; Xie, S. S.; Yuan, H. J.; Yan, X. Q.; Liu, D. F.; Gao, Y.; Zhou, Z. P.; Song, L.; Liu, L. F.; Zhao, X. W.; Dou, X. Y.; Zhou, W. Y.; Wang, G. *Solid State Commun.* **2004**, *131*, 435.
(20) Nikolić, N.; Srećković, T.; Ristić, M. M. *J. Eur. Ceram. Soc.* **2001**, *21*, 2071.
(21) Li, Y.; Ma, X. L. *Phys. Status Solidi A* **2005**, *202*, 435.
(22) Fang, J.; Huang, A.; Zhu, P.; Xu, N.; Xie, J.; Chi, J.; Feng, S.; Xu, R.; Wu, M. *Mater. Res. Bull.* **2001**, *36*, 1391.
(23) Okada, Y.; Tokumaru, Y. *J. Appl. Phys.* **1984**, *56*, 314.
(24) Durig, J. R.; Bush, S. F.; Mercer, E. E. *J. Chem. Phys.* **1966**, *44*, 4238.
(25) Braibanti, A.; Dallavalle, F.; Pellinghelli, M. A.; Leporati, E. *Inorg. Chem.* **1968**, *7*, 1430.